

Near-Atomic-Scale Perspective on the Oxidation of $Ti_3C_2T_x$ MXenes: Insights from Atom Probe Tomography

Mathias Krämer, Bar Favelukis, Ayman A. El-Zoka, Maxim Sokol, Brian A. Rosen, Noam Eliaz, Se-Ho Kim,* and Baptiste Gault*

MXenes are a family of 2D transition metal carbides and nitrides with remarkable properties, bearing great potential for energy storage and catalysis applications. However, their oxidation behavior is not yet fully understood, and there are still open questions regarding the spatial distribution and precise quantification of surface terminations, intercalated ions, and possible uncontrolled impurities incorporated during synthesis and processing. Here, atom probe tomography (APT) analysis of as-synthesized $Ti_3C_2T_x$ MXenes reveals the presence of alkali (Li, Na) and halogen (Cl, F) elements as well as unetched Al. Following oxidation of the colloidal solution of MXenes, it is observed that the alkalis are enriched in TiO_2 nanowires. Although these elements are tolerated through the incorporation by wet chemical synthesis, they are often overlooked when the activity of these materials is considered, particularly during catalytic testing. This work demonstrates how the capability of APT to image these elements in 3D at the near-atomic scale can help to better understand the activity and degradation of MXenes, in order to guide their synthesis for superior functional properties.

1. Introduction

The discovery of MXenes by the Barsoum and Gogotsi groups in 2011 has reignited scientific interest in 2D and layered materials.^[1] To date, numerous MXenes have been synthesized,^[2] and are being intensively studied and tested in applications including supercapacitors and batteries,^[3,4] optoelectronics,^[5] catalysis,^[6] and biosensors or antibacterial membranes.^[7,8] Their properties and performance in various applications are significantly affected by unavoidable surface terminations, denoted by T_x in the chemical formula, which saturate the bare MXene surface during synthesis.^[9] Changes in the electronic properties of the MXenes, for example, have been explained by careful consideration of these functional groups and possible intercalants originating from wet chemical synthesis.^[10] Using them to fine-tune properties would require establishing relationships between activity and their spatial

distribution and concentration, which remain extremely difficult to characterize.


Atom probe tomography (APT) is one of the few techniques that can measure composition in 3D at the near-atomic scale.^[11] In brief, APT relies on the controlled field evaporation of atoms from the apex of a needle-shaped specimen, held in ultra-high vacuum and cryogenic conditions, in the form of individual atomic or molecular ions. By recording the respective time-of-flight and impact coordinates of each ion on a position-sensitive detector, the elemental identity of each ion can be assigned, and the analyzed volume can be reconstructed atom by atom. The combination of these two information allows for 3D compositional mapping with sub-nanometer resolution. In recent years, the application of APT to nanoparticles,^[12–14] nanowires,^[15,16] and nanosheets^[17] has triggered a reckoning that the detailed composition and the presence of trace impurities are of paramount importance when it comes to understanding the activity of nanomaterials.^[18] Impurity elements in the raw materials used during the synthesis may not react at the same rate and hence be preferentially incorporated into the final product,^[17] or may be incorporated into the structure during processing or synthesis by wet chemistry.^[19,20]

M. Krämer, A. A. El-Zoka, S.-H. Kim, B. Gault
Max-Planck-Institut für Eisenforschung
Max-Planck-Straße 1, 40237 Düsseldorf, Germany
E-mail: sehonetkr@korea.ac.kr; b.gault@mpie.de

B. Favelukis, M. Sokol, B. A. Rosen, N. Eliaz
Department of Materials Science and Engineering
Tel Aviv University
P.O. B 39040, Ramat Aviv 6997801, Israel

A. A. El-Zoka, B. Gault
Department of Materials
Royal School of Mines
Imperial College London
London SW7 2AZ, UK

S.-H. Kim
Department of Materials Science and Engineering
Korea University
Seoul 02841, Republic of Korea

 The ORCID identification number(s) for the author(s) of this article can be found under <https://doi.org/10.1002/adma.202305183>

© 2023 The Authors. Advanced Materials published by Wiley-VCH GmbH. This is an open access article under the terms of the Creative Commons Attribution License, which permits use, distribution and reproduction in any medium, provided the original work is properly cited.

DOI: 10.1002/adma.202305183

For MXenes and their surface terminations, most studies to date have relied heavily on X-ray (photoelectron) spectroscopy and electron microscopy techniques for compositional measurements.^[21–25] However, these techniques have certain limitations,^[26] particularly in their ability to accurately detect light elements surrounded by heavy transition metals. For instance, although the detection limit of X-ray photoelectron spectroscopy is typically given as 0.1 to 1 at%, it can exceed 10 at% for light elements surrounded by heavy elements.^[27] In addition, due to the lack of spatial resolution, the detected elements cannot be accurately mapped within the sample. APT, with its compositional sensitivity of a few atomic parts per million for all elements,^[28] can be used to complement these established techniques to address fundamental questions, such as the detailed composition before and after catalytic testing, as has already been shown for several materials other than MXenes.^[29–31]

As the structural and chemical stability of MXenes can also be extremely fragile, APT could also be a tool for better understanding the mechanisms behind the degradation by studying the detailed compositional evolution. MXenes degrade particularly fast in an oxidizing environment (H_2O , O_2 , etc.), leading to their transformation into transition metal oxides.^[32,33] Oxidation, in its early stage, can affect the surface terminations^[34] and thus the properties. For example, an increased concentration of O functional groups results in an increased catalytic activity.^[35] Several studies have demonstrated how further oxidation severely destroys the integrity of the MXene structure, thereby limiting its lifetime in service and precluding many useful applications due to a decrease in the properties of interest.^[36–39] Although efforts have been made to understand the details of their evolving chemistry during oxidation,^[40,41] some questions are still unanswered, such as the role of non-O surface terminations, intercalants, or impurities from synthesis. Designing MXenes with improved oxidation resistance is therefore extremely challenging, and for this reason the improvement of chemical and temperature stability of MXenes is considered in the community to be one of the research challenges of this decade.^[42] Therefore, by providing 3D information with higher detection sensitivity compared to, for example, electron microscopy techniques or X-ray photoelectron spectroscopy, APT could help address this challenge.

In order to further the understanding of the chemical evolution of colloidal $Ti_3C_2T_x$ MXene solution, we introduce here the first APT analyses of as-synthesized MXenes, alongside with the transition metal oxides formed during oxidation. APT revealed the incorporation of alkali (Li, Na) and halogen (Cl, F) elements into the MXene nanosheets, probably inherited from the synthesis. Following oxidation, these elements remained within the newly formed TiO_2 nanowires, indicating that they lowered their free energy and helped to stabilize them. Although most of these elements are considered to be an essential part of the MXenes themselves, these results emphasize that discussions of the activity of MXene-based materials, including throughout oxidation, should take account of them, which are likely to play an important role in the activity^[43] and their resistance to degradation.

2. Results and Discussion

$Ti_3C_2T_x$ MXenes were synthesized by wet chemical etching of the Al layer from a Ti_3AlC_2 MAX phase via the HCl–LiF route

(synthesis of both materials is described in detail in the Supporting Information). In **Figure 1a**, the as-synthesized MXenes shows very clean edges and a defect-free surface, suggesting no major internal defects. Small black dots on the edges may indicate the formation of oxidation products immediately after synthesis. To observe the oxidation of the nanosheets with electron microscopy, the colloidal $Ti_3C_2T_x$ MXene solution was kept at a temperature of 5 °C for about 4 months throughout the oxidation experiment, as described in ref. [44].

Oxidation of the nanosheets in the colloidal solution may have started from the edges due to local structural variations,^[45] where nanoparticles were observed in **Figure 1b**. Previous research has reported the formation of carbon-supported anatase during the oxidation of $Ti_3C_2T_x$ MXenes,^[46] indicating that the nanoparticles formed are TiO_2 . Because atomic vacancies and microstructural defects such as wrinkles are unavoidable in the course of the wet chemical synthesis processes, these preexisting defects on the $Ti_3C_2T_x$ MXene may have created a local electric field that drives the development of the TiO_2 particles by promoting the migration of both Ti cations and electrons.^[47] These pinhole defects then gradually evolved into larger voids, resulting in the degradation and accelerated oxidation of the MXene structure. Zhang et al.^[48] reported that oxidation starts at the defective edges of the MXene sheets and propagates inwards, causing cracks to nucleate and grow. This so-called “scissor effect” shreds the MXene sheets into small pieces and leads to a complete loss of the original structure of the MXene into TiO_2 debris, such as those imaged in **Figure 1c**.

To observe the compositional evolution of the MXenes caused by oxidation for 2 months, dense and sharp needle-shaped APT specimens containing either the as-synthesized or the oxidized $Ti_3C_2T_x$ MXenes were prepared from a nanosheet-metal composite (detailed APT specimen preparation is provided in the Supporting Information). The electrodeposition within a metallic matrix, used as an encapsulating material, increases the success rate and data quality.^[49,50] Here, a Co matrix was used, which, compared to the more commonly used Ni, presents the advantage of having only a single isotope, making it less likely to generate peaks that can obscure the signal from the material of interest in the APT mass spectrum. For example, the use of Ni would cause an unavoidable peak overlap with TiO molecular ions in the APT mass spectrum.^[16]

The reconstructed 3D atom map in **Figure 2a** shows the $Ti_3C_2T_x$ MXene nanosheets with a complex 2D morphology, likely arising from agglomerated or folded nanosheets. These are embedded in Co, shown in yellow. Differences in the evaporation field between the matrix and the nanosheets lead to an irregular curvature of the end surface of the specimen, which results in trajectory aberrations, varying magnification, and intermixing zones in the reconstruction,^[51] as the algorithms do not account for this artifact. An indicative thickness at full width at half maximum of 3.2 nm was obtained by evaluating the Co 1D composition profile in **Figure 2b**. The nominal thickness of a $Ti_3C_2T_x$ monolayer has been reported to be within the order of 1 to 1.5 nm,^[52,53] whereas the interlayer distance between two separate nanosheets can vary depending on the intercalated species.^[54] A single nanosheet or stack of up to three $Ti_3C_2T_x$ nanosheets was hence analyzed.

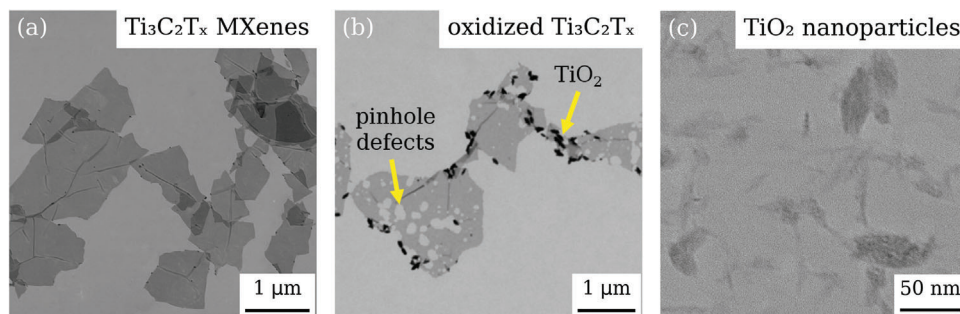


Figure 1. Oxidation processes of the $\text{Ti}_3\text{C}_2\text{T}_x$ MXenes stored in a colloidal solution at 5°C . a) As-synthesized $\text{Ti}_3\text{C}_2\text{T}_x$ MXene nanosheets. b) Oxidized $\text{Ti}_3\text{C}_2\text{T}_x$ MXene after 4 months. c) TiO_2 nanoparticles as products of $\text{Ti}_3\text{C}_2\text{T}_x$ MXene oxidation.

A region of interest, delineated by the dark green-cyan iso-composition surface, encompassing regions in the 3D atom map containing over 6 at% Ti, in Figure 2a, was extracted for compositional analysis. Compared to the nominal value of 1.5, the atomic ratio of Ti to C was measured to be 2.2. Species-specific losses of C have been reported in the APT analysis of carbides,^[55–57] depending on the analysis conditions and partly due to detector saturation associated with two simultaneous impacts of $^{12}\text{C}^+$ ions.^[58] Importantly, it has been questioned whether most MAX phases and their derived MXenes are actually pure carbides or rather oxycarbides.^[59] Therefore, the nominal value may deviate from the 1.5 mentioned above, as O may be present on the C sublattice. Pure carbides may be more resistant to oxidation than oxycarbides, as recent results suggest.^[59,60]

The specimen was analyzed immediately after synthesis; however, a significant amount of O was measured in the material, approximately 46.7 at%. The presence of O can be attributed to synthesis in an aqueous solution, as the highly reactive surface is immediately bonded to, for example, O or OH. Previous reports have shown that under certain controlled high vacuum condi-

tions in the transmission electron microscope the O surface terminations can reach a supersaturation level of 41 at% while retaining the $\text{Ti}_3\text{C}_2\text{T}_x$ MXene nanosheet structure,^[34] and the MXenes directly used from the solution were unlikely to be already oxidized MXenes. However, the measured amount of O was not entirely attributable to O or OH surface terminations. O on the C sublattice,^[59] or weakly bound water molecules to these mentioned surface terminations may also contribute to the increased O content. Besides ion intercalation, intercalation of water molecules is a crucial factor for the aqueous MXene delamination.^[61] Intrinsically hygroscopic cations, such as Li^+ and Na^+ , which were also detected as discussed below, also increase the amount of intercalated water molecules.^[62] Characteristic peaks in the mass spectrum at 17, 18, and 19 Da confirmed the evaporation of H_{1-3}O^+ molecular ions, respectively, while peaks at 81, 82, 83, 84, and 85 Da, partially overlapping with peaks from TiO_2^+ , were attributed to the evaporation of $\text{TiO}(\text{OH})_3^+$. Quantification of the H content was deliberately omitted, as it is known to be extremely challenging from APT to distinguish between H from the analysis chamber and the sample in the form of OH surface

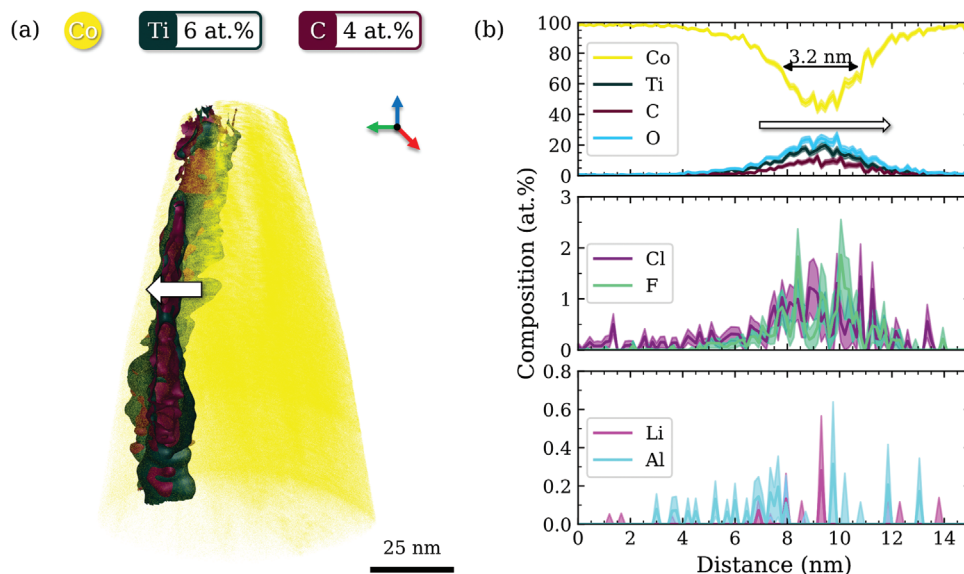


Figure 2. APT analysis of as-synthesized $\text{Ti}_3\text{C}_2\text{T}_x$ MXenes. a) Reconstructed 3D atom map. Agglomerated $\text{Ti}_3\text{C}_2\text{T}_x$ MXene nanosheets are highlighted by a dark green-cyan iso-compositional surface at 6 at% Ti and a reddish-purple iso-compositional surface at 4 at% C. b) 1D compositional profile ($\phi 15\text{ nm} \times 15\text{ nm}$) across the agglomerated MXenes as indicated in (a). Errors are estimated according to counting statistics.

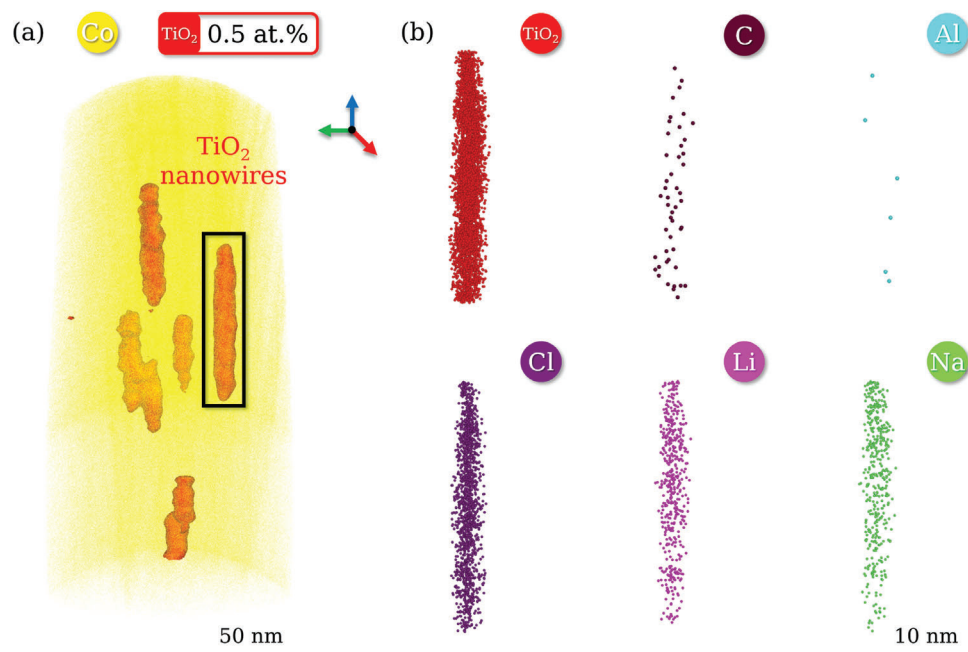


Figure 3. APT analysis of oxidized $\text{Ti}_3\text{C}_2\text{T}_x$ MXenes. a) Reconstructed 3D atom map. TiO_2 nanowires are highlighted by red iso-compositional surfaces at 0.5 at.%. b) Molecular distribution map of TiO_2 and elemental distribution maps of impurity elements in the extracted region of interest indicated in (a).

terminations or intercalated water molecules itself.^[63] In the future, isotopic labeling using heavy water (D_2O) during MXene synthesis may clarify the controversial question of the intrinsic existence of OH terminations on the MXene surface.^[21,64,65]

Not entirely unexpected, several functional surface terminations, intercalated elements, and impurities including Cl, F, Li, Na, and Al were also incorporated and could be quantified within the extracted region of interest of the $\text{Ti}_3\text{C}_2\text{T}_x$ MXenes. The incorporation of Cl and F results from the wet chemical etching process of Al from the precursor MAX phase and the synthesis of delaminated MXenes. High concentrations of HCl and LiF are used in the wet chemical synthesis.^[66,67] Here, the Cl content was measured to be 2.49 at.%. A nearest-neighbor analysis did not indicate the formation of crystalline salts around the $\text{Ti}_3\text{C}_2\text{T}_x$ MXenes, but rather that the as-synthesized MXenes are indeed Cl terminated (see nearest-neighbor analysis in the Supporting Information). Accurate quantification of the amount of F was complicated by the overlapping peaks of F^+ and H_3O^+ in the mass spectrum region at 19 Da, as the naturally abundant isotopes do not allow detailed peak decomposition. However, TiF^{2+} molecular ions were measured (see the mass spectrum in the Supporting Information), so that the F content could be quantified to at least 1.16 at.%. The F content should therefore only be interpreted as a lower limit in the material. Tuning the termination groups on the surface of the MXene may influence its oxidation stability, for instance, Cl-terminated MXenes have been shown to have higher stability than F-terminated MXenes.^[68]

Despite vigorous washing protocols, residuals of Li and Na elements were still present in the analyzed material at 0.02 and 0.11 at.%, respectively. The amount of Na was obtained by means of a peak decomposition with the overlapping peak of $^{46}\text{Ti}^{2+}$ at 23 Da. However, compared to synthesis or processing protocols

where Na is intentionally introduced,^[69] the measured amount is significantly lower. Na likely originated as an impurity in the synthesis chemicals, as was similarly observed for MoS_2 synthesized by wet chemistry.^[17] For example, Na is a known impurity even in high-purity Li salts for battery applications,^[70,71] and here LiF (99%) was used during synthesis. It should be noted that the spatial resolution of APT^[72] does not allow to conclude whether these alkali impurities are on the surface or integrated into the structure of a single-layer MXene. Due to electrostatic effects, these elements could be absorbed on the surface to stabilize it,^[73] or they could spontaneously intercalate between two MXene layers,^[74] as is even desired in the case of Li in the synthesis route used here. The presence of Li or Na atoms on the surface may also directly impact the properties by intercalation doping,^[75] which should grant further targeted investigations.

The complete removal of residual Al atoms is possible by harsh HF etching, often confirmed by X-ray (photoelectron) spectroscopy.^[76] Although the wet etching environment removes the Al layers within the MAX phase by mixing HCl and LiF to form in situ HF, and the desired MXenes were rinsed seven times with deionized water, a trace amount of Al residual atoms at 0.17 at.% was still measured within the $\text{Ti}_3\text{C}_2\text{T}_x$ MXenes.

Figure 3a shows the reconstructed 3D atom map of the transition metal oxides caused by the oxidation of the colloidal $\text{Ti}_3\text{C}_2\text{T}_x$ MXene solution for 2 months. The structures highlighted by red iso-compositional surfaces of 0.5 at.% TiO_2 are similar to those imaged by scanning transmission electron microscopy in Figure 1c, which have a nanowire-like morphology. Their apparent alignment probably arises during electrodeposition in the Co matrix and can be related to the direction of growth of the metallic film, which is not expected to alter their chemistry, since the applied potential is negative (see APT specimen preparation in

the Supporting Information). The atomic ratio of Ti to O within the extracted oxide particle, indicated by the black box, was measured to be 0.54, which is close to the stoichiometric ratio of TiO₂. Dissociation of molecular ions leading to the formation of neutral species such as O₂, whose time-of-flight is no longer proportional to their mass-to-charge ratio,^[77] changes in the acquisition parameters in APT,^[78] or a slight O deficiency could be responsible for the off-stoichiometry of TiO₂. Therefore, assuming that the as-synthesized MXenes are already largely terminated with O, and react with water instead of dissolved O₂,^[79] the oxidation reaction may be simplified in a number of ways, including:

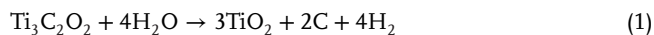


Figure 3b is a close-up of one of these nanowire-like structures with distribution maps of the individually detected elements. The measured impurity contents of Cl, F, Li, and Na were 2.58, 1.62, 0.79, and 0.71 at%, respectively. 54 ± 30 atomic parts per million of Al was collected in the oxidized MXene. Since only 2.09 at% of C was measured in the TiO₂ nanowires, this suggests that the oxidation reaction took place primarily according to Equations (2) and (3), that is, C dissipated in the form of gaseous molecules such as CO₂ and CH₄, rather than forming elemental C.

Overall, the oxidation reaction of the MXene led to an enrichment of alkali elements and a depletion of unetched Al, as visualized in Figure 4. Oxidation of Al to Al₂O₃^[80] may be responsible for the depletion of Al, as the Al₂O₃ and TiO₂ phases have a positive mixing enthalpy,^[81] making the incorporation of Al in the TiO₂ phase unfavorable.^[82] However, fundamental atomistic calculations comparing the stability of the incorporated alkali elements in the MXene and the oxide are missing. While the incorporation of Li into anatase TiO₂ is energetically feasible in general,^[83] Na is a known impurity of TiO₂ synthesized on a soda-lime glass substrate.^[84] Since several Li^[85] and Na titanate derivatives^[86–89] were synthesized by oxidative treatment of Ti₃C₂T_x MXenes with these alkali elements, it is reasonable to assume that they promote the formation of the oxide and stabilize it by lowering the free energy.

Because metal–semiconductor heterostructures can provide rapid separation of photogenerated charge carriers,^[90] Ti₃C₂T_x MXenes were intentionally oxidized to form Ti₃C₂T_x/TiO₂ derivatives for photocatalysis.^[91–94] Other promising applications for these derivatives include electrodes for supercapacitors^[95] and lithium-ion batteries.^[96] However, in our previous report on TiO₂ hollow nanowires, it was pointed out that the lack of precise characterization of impurities has an impact on the laboratory-synthesized TiO₂ properties, which vary and are inconsistent with reported results.^[16] For example, incorporated Na influences the growth and crystallization of TiO₂, and thus the resulting properties.^[84] From this point of view together with the observations made in this study, the alkali elements may have a significant influence on the oxidation mechanism and its kinetics, and consequently also on the properties of the Ti₃C₂T_x/TiO₂ derivatives.

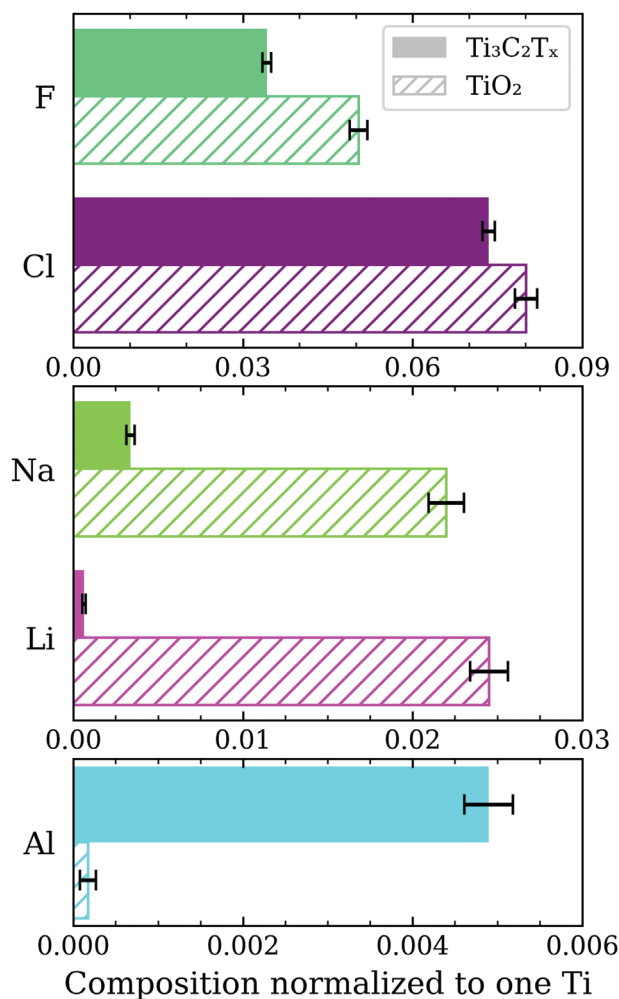


Figure 4. Comparison of the composition of the halogens, alkalis, and Al in the as-synthesized Ti₃C₂T_x MXenes and the TiO₂ nanowires resulting from MXene oxidation. Errors are estimated according to counting statistics. For easier comparability of the data, the compositions were normalized to one Ti (data given in at% are provided in the Supporting Information).

In addition, the detected elements may also work as a dopant for both the as-synthesized Ti₃C₂T_x MXenes and TiO₂ nanowires resulting from MXene oxidation. Doping is a proven and effective engineering strategy to enhance the performance of TiO₂, particularly with alkalis and halogens. For instance, Li-doped TiO₂ has shown significantly improved properties by increasing electronic conductivity, and thus faster electron transport.^[97] Density functional theory calculations predicted an influence of Cl- and F-doping on the band gap of TiO₂^[98] and incorporated Cl shifts the absorption edge to a higher wavelength,^[99] both effects enabling excellent photocatalytic activity. Doping TiO₂ with C can effectively facilitate photogenerated charge transfer and prevent electron–hole recombination.^[100] Surface terminations such as halogens are likely to influence the band structure, as functionalization of Ti₃C₂T_x MXenes with halogens could lead to the formation of Dirac cones near the Fermi level, resulting in semimetallic behavior.^[101] Experimentally, it was observed that

preintercalated Na leads to a reduced diffusion barrier for Na ions and an increased number of active sites due to the increased interlayer spacing of the MXenes.^[102] In summary, both alkali and halogen elements can affect the functional properties of $Ti_3C_2T_x$ MXenes and the TiO_2 nanowires resulting from MXene oxidation. It is therefore essential to study these incorporated elements on the near-atomic scale, for example, using APT.

3. Conclusion

It has been recognized that the methods used to synthesize high-quality MXenes with chemical and structural stability can be critical. We have demonstrated the capability of APT to study the incorporation of alkalis and halogens as surface terminations, intercalated ions, or impurities introduced by the wet chemical synthesis of the MXenes. The alkali elements tended to further concentrate during the oxidation of the $Ti_3C_2T_x$ MXenes to TiO_2 nanowires. Their presence may affect the physical properties of the MXenes themselves, but, importantly, this suggests that the presence and concentration of these elements may contribute to the oxidation mechanism and kinetics, by stabilizing the oxide to the detriment of the MXene itself. In the future, a broader understanding of the influence of these elements may enable targeted utilization to tailor the functional properties of the MXenes and their derived transition metal oxides.

Supporting Information

Supporting Information is available from the Wiley Online Library or from the author.

Acknowledgements

The authors acknowledge financial support from the German Research Foundation (DFG) through DIP Project No. 450800666. S.-H.K. is grateful for supports from KIAT grant funded by the Korea Government (MOTIE, HDR-P0023676) and LINC3.0 funded by NRF Korea. The support from the FIB and APT facilities at MPIE by Uwe Tezins, Andreas Sturm, and Christian Broß is gratefully acknowledged.

Open access funding enabled and organized by Projekt DEAL.

Note: The affiliations were corrected on January 18, 2024, after initial publication online, following a technical error during processing the corrected proof files for Early View publication.

Conflict of Interest

The authors declare no conflict of interest.

Data Availability Statement

The data that support the findings of this study are available from the corresponding author upon reasonable request.

Keywords

2D materials, atom probe tomography, MXenes, nanowires, oxidation

Received: May 31, 2023
Revised: August 17, 2023
Published online: August 22, 2023

- [1] M. Naguib, M. Kurtoglu, V. Presser, J. Lu, J. Niu, M. Heon, L. Hultman, Y. Gogotsi, M. W. Barsoum, *Adv. Mater.* **2011**, *23*, 4248.
- [2] M. Naguib, M. W. Barsoum, Y. Gogotsi, *Adv. Mater.* **2021**, *33*, 2103393.
- [3] B. Anasori, M. R. Lukatskaya, Y. Gogotsi, *Nat. Rev. Mater.* **2017**, *2*, 16098.
- [4] X. Li, Z. Huang, C. E. Shuck, G. Liang, Y. Gogotsi, C. Zhi, *Nat. Rev. Chem.* **2022**, *6*, 389.
- [5] K. Maleski, C. E. Shuck, A. T. Fafarman, Y. Gogotsi, *Adv. Opt. Mater.* **2021**, *9*, 2001563.
- [6] Z. Li, Y. Wu, *Small* **2019**, *15*, 1804736.
- [7] K. Huang, Z. Li, J. Lin, G. Han, P. Huang, *Chem. Soc. Rev.* **2018**, *47*, 5109.
- [8] M. Soleymaniha, M.-A. Shahbazi, A. R. Rafeerad, A. Maleki, A. Amiri, *Adv. Healthcare Mater.* **2019**, *8*, 1801137.
- [9] K. R. G. Lim, M. Shekhirev, B. C. Wyatt, B. Anasori, Y. Gogotsi, Z. W. Seh, *Nat. Synth.* **2022**, *1*, 601.
- [10] J. L. Hart, K. Hantanasirisakul, A. C. Lang, B. Anasori, D. Pinto, Y. Pivak, J. T. van Ommen, S. J. May, Y. Gogotsi, M. L. Taheri, *Nat. Commun.* **2019**, *10*, 522.
- [11] B. Gault, A. Chiaramonti, O. Cojocaru-Mirédin, P. Stender, R. Dubosq, C. Freysoldt, S. K. Mäkinen, T. Li, M. Moody, J. M. Cairney, *Nat. Rev. Methods Primers* **2021**, *1*, 51.
- [12] K. Tedsree, T. Li, S. Jones, C. W. A. Chan, K. M. K. Yu, P. A. J. Bagot, E. A. Marquis, G. D. W. Smith, S. C. E. Tsang, *Nat. Nanotechnol.* **2011**, *6*, 302.
- [13] T. Li, P. A. J. Bagot, E. Christian, B. R. C. Theobald, J. D. B. Sharman, D. Ozkaya, M. P. Moody, S. C. E. Tsang, G. D. W. Smith, *ACS Catal.* **2014**, *4*, 695.
- [14] P. Felfer, P. Benndorf, A. Masters, T. Maschmeyer, J. M. Cairney, *Angew. Chem., Int. Ed.* **2014**, *53*, 11190.
- [15] D. E. Perea, J. E. Allen, S. J. May, B. W. Wessels, D. N. Seidman, L. J. Lauhon, *Nano Lett.* **2006**, *6*, 181.
- [16] J. Lim, S.-H. Kim, R. A. Armengol, O. Kasian, P.-P. Choi, L. T. Stephenson, B. Gault, C. Scheu, *Angew. Chem., Int. Ed.* **2020**, *59*, 565.
- [17] S.-H. Kim, J. Lim, R. Sahu, O. Kasian, L. T. Stephenson, C. Scheu, B. Gault, *Adv. Mater.* **2020**, *32*, 1907235.
- [18] T. Li, A. Devaraj, N. Kruse, *Cell Rep. Phys. Sci.* **2022**, *3*, 101188.
- [19] S.-H. Kim, S.-H. Yoo, P. Chakraborty, J. Jeong, J. Lim, A. A. El-Zoka, X. Zhou, L. T. Stephenson, T. Hickel, J. Neugebauer, C. Scheu, M. Todorova, B. Gault, *J. Am. Chem. Soc.* **2022**, *144*, 987.
- [20] S.-H. Kim, S.-H. Yoo, S. Shin, A. A. El-Zoka, O. Kasian, J. Lim, J. Jeong, C. Scheu, J. Neugebauer, H. Lee, M. Todorova, B. Gault, *Adv. Mater.* **2022**, *34*, 2203030.
- [21] V. Natu, M. Benchakar, C. Canaff, A. Habrioux, S. Célérier, M. W. Barsoum, *Matter* **2021**, *4*, 1224.
- [22] H. Alnoor, A. Elskova, J. Palisaitis, I. Persson, E. Tseng, J. Lu, L. Hultman, P. Persson, *Mater. Today Adv.* **2021**, *9*, 100123.
- [23] V. Natu, J. L. Hart, M. Sokol, H. Chiang, M. L. Taheri, M. W. Barsoum, *Angew. Chem., Int. Ed.* **2019**, *58*, 12655.
- [24] Y. Lee, S. J. Kim, Y.-J. Kim, Y. Lim, Y. Chae, B.-J. Lee, Y.-T. Kim, H. Han, Y. Gogotsi, C. W. Ahn, *J. Mater. Chem. A* **2020**, *8*, 573.
- [25] P. H. Nguyen, D. H. Nguyen, D. Kim, M. K. Kim, J. Jang, W. H. Sim, H. M. Jeong, G. Namkoong, M. S. Jeong, *ACS Appl. Mater. Interfaces* **2022**, *14*, 51487.
- [26] M. Shekhirev, C. E. Shuck, A. Sarycheva, Y. Gogotsi, *Prog. Mater. Sci.* **2021**, *120*, 100757.
- [27] A. G. Shard, *Surf. Interface Anal.* **2014**, *46*, 175.
- [28] D. Haley, A. J. London, M. P. Moody, *Microsc. Microanal.* **2020**, *26*, 964.
- [29] T. Li, O. Kasian, S. Cherevko, S. Zhang, S. Geiger, C. Scheu, P. Felfer, D. Raabe, B. Gault, K. J. J. Mayrhofer, *Nat. Catal.* **2018**, *1*, 300.

- [30] W. Xiang, N. Yang, X. Li, J. Linnemann, U. Hagemann, O. Ruediger, M. Heidelmann, T. Falk, M. Aramini, S. DeBeer, M. Muhler, K. Tschulik, T. Li, *Nat. Commun.* **2022**, *13*, 179.
- [31] L. S. Aota, C. Jung, S. Zhang, S.-H. Kim, B. Gault, *ACS Energy Lett.* **2023**, *8*, 2824.
- [32] A. Iqbal, J. Hong, T. Y. Ko, C. M. Koo, *Nano Converg.* **2021**, *8*, 9.
- [33] J. Jiang, S. Bai, J. Zou, S. Liu, J.-P. Hsu, N. Li, G. Zhu, Z. Zhuang, Q. Kang, Y. Zhang, *Nano Res.* **2022**, *15*, 6551.
- [34] I. Persson, J. Halim, T. W. Hansen, J. B. Wagner, V. Darakchieva, J. Palisaitis, J. Rosen, P. O. Å. Persson, *Adv. Funct. Mater.* **2020**, *30*, 1909005.
- [35] G. Gao, A. P. O'Mullane, A. Du, *ACS Catal.* **2017**, *7*, 494.
- [36] F. Cao, Y. Zhang, H. Wang, K. Khan, A. K. Tareen, W. Qian, H. Zhang, H. Ågren, *Adv. Mater.* **2022**, *34*, 2107554.
- [37] X. Li, Z. Huang, C. Zhi, *Front. Mater.* **2019**, *6*, 312.
- [38] H. Liang, J. Liu, *ChemCatChem* **2022**, *14*, 202101375.
- [39] A. Bhat, S. Anwer, K. S. Bhat, M. I. H. Mohideen, K. Liao, A. Qurashi, *npj 2D Mater. Appl.* **2021**, *5*, 61.
- [40] H. Ghassemi, W. Harlow, O. Mashtalir, M. Beidaghi, M. R. Lukatskaya, Y. Gogotsi, M. L. Taheri, *J. Mater. Chem. A* **2014**, *2*, 14339.
- [41] K. Badawy, K. Liao, N. Singh, *ACS Appl. Nano Mater.* **2022**, *5*, 16731.
- [42] Y. Gogotsi, Q. Huang, *ACS Nano* **2021**, *15*, 5775.
- [43] O. Westhead, R. Jervis, I. E. L. Stephens, *Science* **2021**, *372*, 1149.
- [44] Y. Chae, S. J. Kim, S.-Y. Cho, J. Choi, K. Maleski, B.-J. Lee, H.-T. Jung, Y. Gogotsi, Y. Lee, C. W. Ahn, *Nanoscale* **2019**, *11*, 8387.
- [45] L. H. Karlsson, J. Birch, J. Halim, M. W. Barsoum, P. O. Å. Persson, *Nano Lett.* **2015**, *15*, 4955.
- [46] M. Naguib, O. Mashtalir, M. R. Lukatskaya, B. Dyatkin, C. Zhang, V. Presser, Y. Gogotsi, M. W. Barsoum, *Chem. Commun.* **2014**, *50*, 7420.
- [47] F. Xia, J. Lao, R. Yu, X. Sang, J. Luo, Y. Li, J. Wu, *Nanoscale* **2019**, *11*, 23330.
- [48] C. J. Zhang, S. Pinilla, N. McEvoy, C. P. Cullen, B. Anasori, E. Long, S.-H. Park, A. Seral-Ascaso, A. Shmeliov, D. Krishnan, C. Morant, X. Liu, G. S. Duesberg, Y. Gogotsi, V. Nicolosi, *Chem. Mater.* **2017**, *29*, 4848.
- [49] S.-H. Kim, P. W. Kang, O. O. Park, J.-B. Seol, J.-P. Ahn, J. Y. Lee, P.-P. Choi, *Ultramicroscopy* **2018**, *190*, 30.
- [50] H. Jun, K. Jang, C. Jung, P.-P. Choi, *Microsc. Microanal.* **2021**, *27*, 1007.
- [51] M. K. Miller, *J. Phys., Colloq.* **1987**, *48*, 565.
- [52] X. Wang, X. Shen, Y. Gao, Z. Wang, R. Yu, L. Chen, *J. Am. Chem. Soc.* **2015**, *137*, 2715.
- [53] A. Lipatov, M. Alhabeab, M. R. Lukatskaya, A. Bosen, Y. Gogotsi, A. Sinitskii, *Adv. Electron. Mater.* **2016**, *2*, 1600255.
- [54] A. Lipatov, H. Lu, M. Alhabeab, B. Anasori, A. Gruverman, Y. Gogotsi, A. Sinitskii, *Sci. Adv.* **2018**, *4*, eaat0491.
- [55] M. Thuvander, J. Weidow, J. Angseryd, L. Falk, F. Liu, M. Sonestedt, K. Stiller, H.-O. Andrén, *Ultramicroscopy* **2011**, *111*, 604.
- [56] Z. Peng, F. Vurpillot, P.-P. Choi, Y. Li, D. Raabe, B. Gault, *Ultramicroscopy* **2018**, *189*, 54.
- [57] S. Ndiaye, C. Bacchi, B. Klaes, M. Canino, F. Vurpillot, L. Rigutti, *J. Phys. Chem. C* **2023**, *127*, 5467.
- [58] Z. Peng, D. Zanuttini, B. Gervais, E. Jacquet, I. Blum, P.-P. Choi, D. Raabe, F. Vurpillot, B. Gault, *J. Phys. Chem. Lett.* **2019**, *10*, 581.
- [59] P. P. Michałowski, M. Anayee, T. S. Mathis, S. Kozdra, A. Wójcik, K. Hantanasirisakul, I. Józwiak, A. Piątkowska, M. Możdzonek, A. Malinowska, R. Diduszko, E. Wierzbicka, Y. Gogotsi, *Nat. Nanotechnol.* **2022**, *17*, 1192.
- [60] T. S. Mathis, K. Maleski, A. Goad, A. Sarycheva, M. Anayee, A. C. Foucher, K. Hantanasirisakul, C. E. Shuck, E. A. Stach, Y. Gogotsi, *ACS Nano* **2021**, *15*, 6420.
- [61] M. Alhabeab, K. Maleski, B. Anasori, P. Lelyukh, L. Clark, S. Sin, Y. Gogotsi, *Chem. Mater.* **2017**, *29*, 7633.
- [62] N. Shpigel, M. D. Levi, S. Sigalov, T. S. Mathis, Y. Gogotsi, D. Aurbach, *J. Am. Chem. Soc.* **2018**, *140*, 8910.
- [63] Y.-S. Chen, P.-Y. Liu, R. Niu, A. Devaraj, H.-W. Yen, R. K. W. Marceau, J. M. Cairney, *Microsc. Microanal.* **2022**, *29*, 1.
- [64] P. Persson, J. Rosen, *Curr. Opin. Solid State Mater. Sci.* **2019**, *23*, 100774.
- [65] L.-Å. Näslund, I. Persson, *Appl. Surf. Sci.* **2022**, *593*, 153442.
- [66] M. Ghidui, M. R. Lukatskaya, M.-Q. Zhao, Y. Gogotsi, M. W. Barsoum, *Nature* **2014**, *516*, 78.
- [67] Y.-J. Kim, S. J. Kim, D. Seo, Y. Chae, M. Anayee, Y. Lee, Y. Gogotsi, C. W. Ahn, H.-T. Jung, *Chem. Mater.* **2021**, *33*, 6346.
- [68] J. Lu, I. Persson, H. Lind, J. Palisaitis, M. Li, Y. Li, K. Chen, J. Zhou, S. Du, Z. Chai, Z. Huang, L. Hultman, P. Eklund, J. Rosen, Q. Huang, P. O. Persson, *Nanoscale Adv.* **2019**, *1*, 3680.
- [69] M. Ghidui, J. Halim, S. Kota, D. Bish, Y. Gogotsi, M. W. Barsoum, *Chem. Mater.* **2016**, *28*, 3507.
- [70] L. Fu, H. Xie, J. Huang, X. Chen, L. Chen, *Spectrochim. Acta, Part B* **2021**, *181*, 106217.
- [71] R. Merrifield, *Determination of Impurities in Lithium Materials with the NexION 5000 ICP-MS*, Application Note. PerkinElmer Inc., Waltham, MA, USA **2021**.
- [72] B. Gault, B. Klaes, F. F. Morgado, C. Freysoldt, Y. Li, F. De Geuser, L. T. Stephenson, F. Vurpillot, *Microsc. Microanal.* **2022**, *28*, 1116.
- [73] S. Doo, A. Chae, D. Kim, T. Oh, T. Y. Ko, S. J. Kim, D.-Y. Koh, C. M. Koo, *ACS Appl. Mater. Interfaces* **2021**, *13*, 22855.
- [74] M. R. Lukatskaya, O. Mashtalir, C. E. Ren, Y. Dall'Agnese, P. Rozier, P. L. Taberna, M. Naguib, P. Simon, M. W. Barsoum, Y. Gogotsi, *Science* **2013**, *341*, 1502.
- [75] J. Wan, S. D. Lacey, J. Dai, W. Bao, M. S. Fuhrer, L. Hu, *Chem. Soc. Rev.* **2016**, *45*, 6742.
- [76] E. Saita, M. Iwata, Y. Shibata, Y. Matsunaga, R. Suizu, K. Awaga, J. Hirotsu, H. Omachi, *Front. Chem.* **2022**, *10*, 841313.
- [77] B. Gault, D. W. Saxey, M. W. Ashton, S. B. Sinnott, A. N. Chiaramonti, M. P. Moody, D. K. Schreiber, *New J. Phys.* **2016**, *18*, 033031.
- [78] R. Verberne, D. W. Saxey, S. M. Reddy, W. D. A. Rickard, D. Fougereuse, C. Clark, *Microsc. Microanal.* **2019**, *25*, 539.
- [79] S. Huang, V. N. Mochalin, *Inorg. Chem.* **2019**, *58*, 1958.
- [80] Y. Xie, Y. Dall'Agnese, M. Naguib, Y. Gogotsi, M. W. Barsoum, H. L. Zhuang, P. R. C. Kent, *ACS Nano* **2014**, *8*, 9606.
- [81] J. Zheng, X. Hu, Z. Ren, X. Xue, K. Chou, *ISIJ Int.* **2017**, *57*, 1762.
- [82] M.-K. Sun, I.-H. Jung, H.-G. Lee, *Met. Mater. Int.* **2008**, *14*, 791.
- [83] F. Tielens, M. Calatayud, A. Beltrán, C. Minot, J. Andrés, *J. Electroanal. Chem.* **2005**, *581*, 216.
- [84] H. Xie, N. Li, B. Liu, J. Yang, X. Zhao, *J. Phys. Chem. C* **2016**, *120*, 10390.
- [85] J. Wang, S. Dong, H. Li, Z. Chen, S. Jiang, L. Wu, X. Zhang, *J. Electroanal. Chem.* **2018**, *810*, 27.
- [86] Y. Dong, Z.-S. Wu, S. Zheng, X. Wang, J. Qin, S. Wang, X. Shi, X. Bao, *ACS Nano* **2017**, *11*, 4792.
- [87] J. Huang, R. Meng, L. Zu, Z. Wang, N. Feng, Z. Yang, Y. Yu, J. Yang, *Nano Energy* **2018**, *46*, 20.
- [88] C. Zeng, F. Xie, X. Yang, M. Jaroniec, L. Zhang, S.-Z. Qiao, *Angew. Chem., Int. Ed.* **2018**, *57*, 8540.
- [89] W. Zhong, M. Tao, W. Tang, W. Gao, T. Yang, Y. Zhang, R. Zhan, S.-J. Bao, M. Xu, *Chem. Eng. J.* **2019**, *378*, 122209.
- [90] L. Yuan, Z. Geng, J. Xu, F. Guo, C. Han, *Adv. Funct. Mater.* **2021**, *31*, 2101103.
- [91] J. Low, L. Zhang, T. Tong, B. Shen, J. Yu, *J. Catal.* **2018**, *361*, 255.

- [92] J. Chen, H. Zheng, Y. Zhao, M. Que, W. Wang, X. Lei, *Ceram. Int.* **2020**, *46*, 20088.
- [93] S. Debow, T. Zhang, X. Liu, F. Song, Y. Qian, J. Han, K. Maleski, Z. B. Zander, W. R. Creasy, D. L. Kuhn, Y. Gogotsi, B. G. DeLacy, Y. Rao, *J. Phys. Chem. C* **2021**, *125*, 10473.
- [94] J. Vida, P. Gemeiner, M. Pavličková, M. Mazalová, P. Souček, D. Plašienka, T. Homola, *Nanoscale* **2023**, *15*, 1289.
- [95] M. Cao, F. Wang, L. Wang, W. Wu, W. Lv, J. Zhu, *J. Electrochem. Soc.* **2017**, *164*, A3933.
- [96] Y. Jia, J. Liu, L. Shang, *Ionics* **2023**, *29*, 531.
- [97] R. Teimouri, Z. Heydari, M. P. Ghaziani, M. Madani, H. Abdy, M. Kolahdouz, E. Asl-Soleimani, *Superlattices Microstruct.* **2020**, *145*, 106627.
- [98] P.-P. Filippatos, N. Kelaidis, M. Vasilopoulou, D. Davazoglou, N. N. Lathiotakis, A. Chroneos, *Sci. Rep.* **2019**, *9*, 19970.
- [99] X.-K. Wang, C. Wang, W.-Q. Jiang, W.-L. Guo, J.-G. Wang, *Chem. Eng. J.* **2012**, *189-190*, 288.
- [100] X. Han, L. An, Y. Hu, Y. Li, C. Hou, H. Wang, Q. Zhang, *Appl. Catal., B* **2020**, *265*, 118539.
- [101] M. Faraji, A. Bafekry, M. M. Fadlallah, F. Molaei, N. N. Hieu, P. Qian, M. Ghergherehchi, D. Gogova, *Phys. Chem. Chem. Phys.* **2021**, *23*, 15319.
- [102] J. Luo, C. Fang, C. Jin, H. Yuan, O. Sheng, R. Fang, W. Zhang, H. Huang, Y. Gan, Y. Xia, C. Liang, J. Zhang, W. Li, X. Tao, *J. Mater. Chem. A* **2018**, *6*, 7794.